STScI | SPACE TELESCOPE SCIENCE INSTITUTE

Instrument Science Report WFC3 2023-04

UVIS Shutter Timing Jitter

K. Huynh & P.R. McCullough

August 14, 2023

Abstract

Timing Jitter in the WFC3/UVIS shutter is the non-repeatability in the exposure times from one exposure to another. We determine the timing jitter of the UVIS shutter from a series of G280 spectra taken in one HST orbit of calibration program 17265. The actual exposure time varies by 2.43 ± 0.32 ms, for exposures with nominal lengths of 1-s, 2-s, and 4-s. The shutter exceeds its specification for repeatability (10 ms) by a factor of four. The jitter is approximately ten times smaller than our reported value for 0.5-s exposures, in which the shutter sweeps without stopping during its open state. On the other hand, the jitter for 0.7-s exposures is about double the reported value. The 0.7-s exposure is the shortest one with a temporary stop in the open state, and as a result is most affected by the vibration of the shutter system. The shutter's tendency to vibrate more for blade B than blade A does not affect the timing jitter noticeably. The spectra, obtained on the UVIS 2 CCD, exhibit a small loss of charge associated with saturation.

Introduction

The repeatability of the UVIS exposure time is a characteristic of the mechanical shutter: a rotating, pizza-sized, circular metal blade with two openings that transmit light in between two areas of metal that block light (cf. Figure 1 of Kurtz et al. 2018). For exposure times greater than or equal to 0.7-s, the shutter accelerates up to speed, continues rotating, and then decelerates to a stop, leaving the shutter in one of its two open positions (A or B). The process is repeated after a specified interval in order to close the shutter. For half second exposures, the shutter blade instead makes a continuous sweep from one closed position to another without resting in between (Hilbert 2010).

The shutter's operation defines the exposure time, but idiosyncrasies of the mechanical shutter results in slight non-repeatability in the exposure time from one exposure to another, which we refer to as "shutter timing jitter" or simply "jitter." The system requirements include a repeatability to 0.010-s (Hilbert 2010) and on-orbit tests have been interpreted as A) that the UVIS shutter does not quite satisfy the requirement, or B) passes it with margin.

Photometric variability in repeated direct images of the standard star GD153 in 0.5-s to 1-s exposures were interpreted as 9 to 12 ms of timing jitter (Hilbert 2010, Table 5).[1] With better flat fields, Sahu et al. (2015) reduced the imagery from Program 14019, that was previously analyzed by Hilbert, as well as similar data from Program 11427. They obtained similar results for the photometric variation in time series of short exposures of various lengths.[2] However, data reduction of direct images depends critically on the dot product of the stellar image's light distribution (often referred to as the point spread function, or PSF) with the appropriate flat field, which itself is prone to measurement error of a fraction of a percent.

Hilbert 2004 estimated the shutter timing jitter as a root mean square (r.m.s) value of 0.006-s using the photometric repeatability of short internal flat field exposure sets (0.7-- 4-s) illuminated by the XE lamp.[3] We derive a 0.0035-s r.m.s. timing jitter from more than a hundred "bowtie" flat fields obtained in orbit with 1.0-s exposures (see Appendix A for details on "bowtie" flat fields and the derivation of the timing jitter). However, the mechanical vibration associated with shutter operation may invalidate such a method because it could create genuine photometric variation of the lamp or affect the coupling of the lamp to the CCD. As a consequence, we interpret both the 0.006-s result obtained in the 1-g environment and the 0.0035-s result obtained in the 0-g environment as *upper limits*.

From measurements of stars scanned rapidly across the CCD, the vibration induced by the shutter motion is known to last at least 0.7-s and is greater in amplitude for blade B than blade A (cf. Figure 15 of Kurtz et al. 2018). The spectra analyzed in this report also exhibit more vibration for blade B than blade A, but our photometric analysis is not affected by the variation in the blurring of the spectral lines, because while the flux is *redistributed* on the CCD, it is *conserved*. That is, the throughput from the star to the CCD is apparently not affected as it is from the internal lamp to the CCD.

In the test described in this report, we observe a spectrophotometric standard star with the G280 grism in order to disperse its light across hundreds of pixels. This allows for high photometric precision in very short exposures so we can more precisely measure the shutter timing jitter compared to the previously mentioned results from direct images of a star or an internal flat field. This program was designed to minimize the Poisson noise of the detected photons, the CCD amplifier's read noise, the sporadic hits of cosmic rays, effects of saturation, and other noise. Doing so ensures that the shutter timing jitter dominates the contributions to observation variability (cf. Analysis).

[1] Throughout this report, we will describe exposure times as 0.5-s, 0.7-s, 1-s, 2-s, and 4-s, while recognizing that those commanded exposure times differ from the actual exposure times.

[2] We re-analyzed photometric tables corresponding to Figure 6 of Sahu et al. 2015 provided by private communication from Sahu.

[3] We analyzed the third columns of Hilbert's Tables 6 and 7 separately; both implied timing jitter of 0.006-s r.m.s.

Data

Spectra of the spectrophotometric standard star HR-5501 were collected in a single orbit with commanded exposure times of 0.5, 0.7, 1.0, 2.0, and 4.0 seconds to measure the non-repeatability of the mechanical shutter under Program 17265.[4] We define a 2250×340 subarray centered on UVIS 2 to record both positive and negative orders for greater dynamic range. There are six exposures per commanded exposure time, all unflashed, with the exception of 2.0-s exposures, for which ten iterations of pairs of exposures were commanded, with and without flash of 20 electrons per pixel. All exposures went through standard calibration by `calwf3` version 3.6.2[5] without charge transfer efficiency (CTE) correction and were downloaded from the Mikulski Archive for Space Telescopes (MAST).

A sample 0.5-s exposure is shown in Figure 1. No pixels were saturated in the 0.5-s exposures, except in the zeroth order, which is heavily saturated. The dispersion is ∼1.4 nm per column in first order, and the short-wavelength cutoff to the sensitivity is ∼200 nm. Integrated over the positive orders, the spectrum has 70 million photoelectrons s^{-1}, which is 10,000 times greater than the F395N direct images of the star GD 153 in calibration programs 11427 and 14019 mentioned in the Introduction. Figure 2 shows the sums of each column in the longest exposure (4-s), illustrating the locations of the Balmer absorption lines in the B9.5V star's spectrum and the greater than a million photoelectrons per column in the peak of the positive orders. Figure 3 maps the pixels that were marked as saturated in the DQ array of exposures of various lengths. For the longest exposures (4-s), 250 to 350 columns had at least one saturated pixel in the negative or positive orders, respectively, and at most, ∼15 pixels were saturated per column.

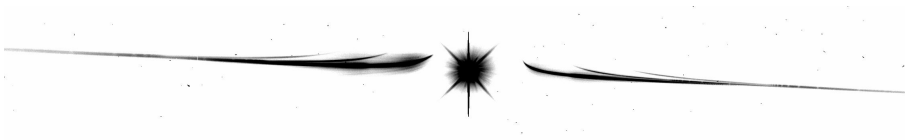

Figure 1: *Sample 0.5-s G280 exposure from Program 17265, displayed with logarithmic scaling. The positive orders (left) are exposed ∼3 times more than the negative orders (right). The zeroth order is the overexposed center signal with four diagonal diffraction spikes and vertical bleed trails both above and below.*

[4]Program 17265 consists of two visits. The first visit missed the original target HR-7596 (V=6.53, A0III) due to user error. A second visit was added to correct the error and the target was switched to HR-5501 (V = 5.665, B9.5V) due to scheduling availability.

[5]See `hstcal` release 2.7.2 (`https://github.com/spacetelescope/hstcal/releases/tag/2.7.2`), which includes updates for `calwf3` 3.6.2.

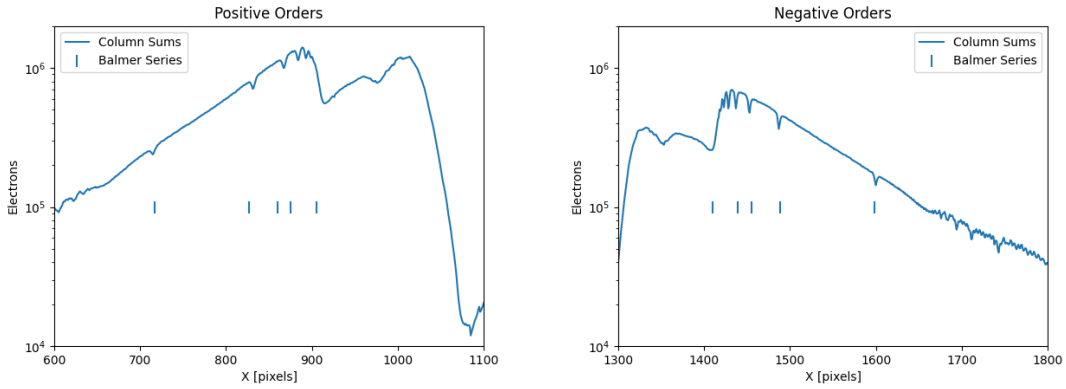

Figure 2: *Sums of each column in positive orders (left) and negative orders (right) from a 4.0-s exposure (PID 17265). The approximate positions of four Balmer lines and the Balmer break are indicated by five vertical bars at 656 nm, 486 nm, 434 nm, 410 nm, and 365 nm, respectively. The farther from the zeroth order at X=1162, the longer the wavelength.*

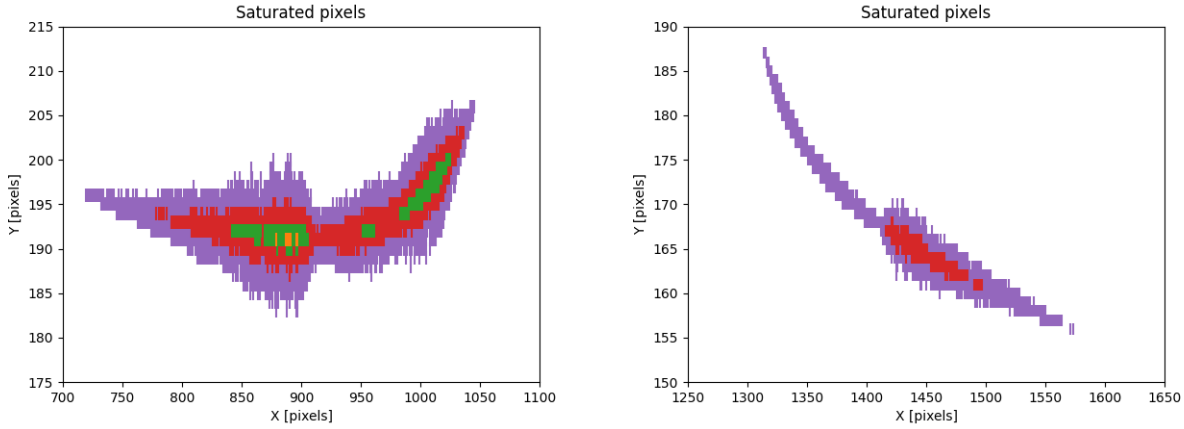

Figure 3: *Saturated pixels in positive orders (left) and negative orders (right) of the G280 exposure (PID 17265). The vertical scale is exaggerated 10x compared to the horizontal scale. Pixels are colored purple, red, green, and orange for 4.0-s, 2.0-s, 1.0-s, and 0.7-s respectively. The 0.5-s exposures saturated zero pixels.*

Analysis

Our usage of the G280 grism to spread high counts of the bright HR-5501 star across a subarray in short exposures was designed in this manner so that the shutter jitter would dominate all other sources contributing to the nonrepeatability of the photometry. In this section we discuss each potential source of photometric noise: shutter jitter, poisson noise, read noise, cosmic rays, and flash. We do not address charge transfer efficiency (CTE) except

in so far as flash may affect it.

Sources of Noise

The **shutter jitter** is the non-repeatability of the effective exposure time from one exposure to another and is associated with the mechanical shutter sweeping across the focal plane in a manner that is not precisely repeatable. We model the detection of photons as a Poisson process with constant photon rate R and integration time $T + e_t$, where T is the mean exposure time and e_t is an error term associated with the shutter's timing jitter. We model the distribution of e_t as normal (Gaussian) with width σ_t; later, we show its shape is indeed approximately Gaussian.

The purpose of this study is to determine σ_t from a series of observations of G280 spectra taken with exposures of various commanded durations. Because the mean number of detected photons is very large for our observations, we approximate the **Poisson** variable as a normal (Gaussian) distribution, with a mean value equal to the product of the photon rate and the mean exposure time ($R \times T$), and two independent error components: A) the Poisson error (σ_p), and B) the photometric error associated with timing jitter (σ_j). Stated in terms of fractional errors for a nominal exposure time T, these terms are:

$$\sigma_p = \frac{1}{\sqrt{R * T}} \tag{1}$$

and

$$\sigma_j = \frac{\sigma_t}{T} \tag{2}$$

For these G280 observations, the rate of photoelectrons is R=7E7 photons s^{-1} summed over the positive orders, and is approximately half as much for the negative orders (Table 3 in the Appendix). Thus the Poisson noise of either sum is much less than the anticipated shutter timing jitter. For example, we later estimate $\sigma_t \approx 0.002$-s, so we anticipate that successive exposures with $T = 2.0$-s will exhibit apparent flux variability from one exposure to the next of ∼1000 ppm (shutter jitter) and only ∼85 ppm (Poisson) for the positive orders.

The **read noise** is even smaller than the Poisson noise. The CCD's amplifier D has 3.18-e r.m.s. read noise per pixel (FITS keyword READNSED). For an aperture large enough to contain the positive orders, e.g. ∼100 rows by ∼1000 columns, the variance attributable to read noise (σ_{rn}^2) would be 1E6, i.e. 100x1000x3.18^2, which is much less than the variance attributable to Poisson noise, 7E7 * T.

The effect of random **cosmic ray** hits is also expected to be very small. First we identified pixels affected by cosmic rays in each individual exposure as those pixels whose deviation from their temporal median value is ten times larger than the value stored in their error array. We then replace those pixels with that particular pixel's median value from all images of that same exposure time. This method works superbly in "sky" regions, but does not adequately address cosmic ray affecting the spectral trace. Thus, we estimate the expected number of electrons from cosmic ray hit(s) superposed upon the bright part of the spectral trace which our technique may have missed. The rate of cosmic ray hits is ∼1 hit per cm^2 s^{-1} with a typical hit corresponding to ∼2500 electrons (Miles et al. 2021). For our observations, the longest commanded exposure times are 4-s. However, cosmic rays also hit the CCD during

the time an exposure is being read out (28-s for these custom subarrays). The UVIS CCD pixels are 15 microns by 15 microns. Thus, we anticipate ∼1 cosmic ray hit unidentified in an area near the bright spectral trace of, say, 15 pixels by 1000 pixels. One overlooked cosmic ray (∼2500 electrons) divided by the star's flux in the positive orders, would equal 2500 / (7E7 * T), or (36 / T) ppm. Hence, the noise due to cosmic rays overlooked near the spectral trace, would be less than that of Poisson noise, and again, much smaller than the shutter jitter.

The LED **flash** is superposed on half of the 2.0-s exposures. Because each pixel would detect a Poisson random number of electrons with a mean value of 20 electrons (and thus the variance attributable to the flash is also 20 electrons), the flash variance is also negligible compared to the Poisson noise of the stellar spectrum and hence much less than the shutter jitter noise. Any variability of the LED from one exposure to another would have been accounted for by our sky subtraction performed on each individual exposure.

For each given exposure time, we analyze a series of N identical observations.[6] From any series of N observations, we calculate a mean and a standard deviation. By dividing the standard deviation by the mean, we obtain the fractional photometric uncertainty of the measurements in that particular series. The root mean square (r.m.s.) precision of the standard deviation is dependent on the number N: as N increases, estimates of the standard deviation becomes more precise. The fractional uncertainty u/σ_t of the standard deviation σ_t from a finite series of N observations is[7]

$$\frac{u}{\sigma_t} \approx \frac{1}{\sqrt{2(N-1)}} \tag{3}$$

which is 0.32 for N=6 or 0.24 for N=10.[8] As explained later, after disregarding the two series with exposure times less than 1-s, we have four series, two with N=6 and two with N=10, so in principle we could expect to determine σ_t to 32%, 32%, 24%, and 24% from each series individually, or to 13% in total.

Measuring Timing Jitter

We measure the total counts in the positive and negative orders of the G280 spectra using an automated traced aperture created with the 0.5-s median stack exposure through the `skimage` package in `python`. The aperture is created by connecting adjacent points above a background-masking threshold, creating several regions. We find the two largest regions by area, which are the positive and negative order spectra due to the large number of pixels of high counts. We then sum the total counts in each aperture separately. We choose to include all of the orders rather than just the positive first order (+1) and the negative first order (−1) because we are more concerned about collecting as much counts as possible to increase the precision of our timing jitter measurement rather than the accuracy of the spectrophotometry. To account for counts bleeding out of the aperture at higher exposure

[6] N=6 each for the series of 0.5-,0.7-,1.0- and 4.0- second exposures. We made two series of 2 s exposures, interleaved, with N=10 for each of the flashed and unflashed exposures (cf. Table 3 in Appendix B).

[7] `https://web.eecs.umich.edu/~fessler/papers/files/tr/stderr.pdf`

[8] In Equation 3 the variable is an Arabic u, for uncertainty, not a Greek μ often used for a mean value.

times due to saturation, we increase the size of the traced aperture by 20 pixels above and below the edge of the region. Figure 4 shows a sample 4.0-s exposure covered by the traced region, as well as the same exposure with the trace region extended above and below by an additional 20 rows in order to account for the effects of saturation on pixels bleeding out of the original aperture.

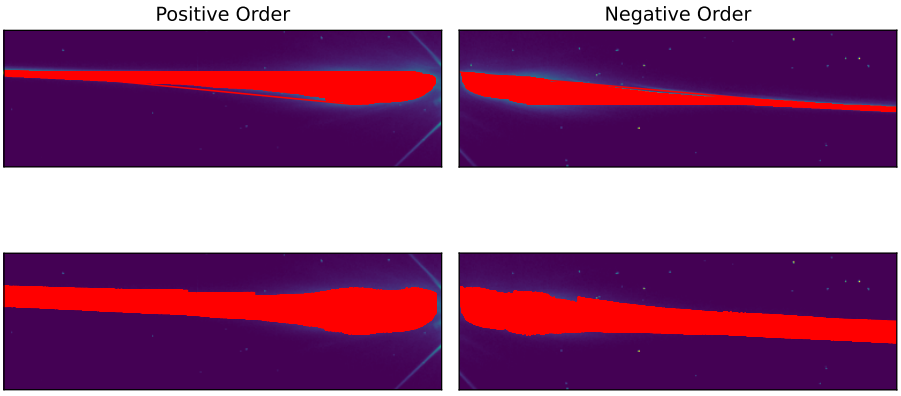

Figure 4: *Sample 4.0-se exposure from PID 17265 with the traced aperture plotted on top of the positive and negative spectrum order. Top: original traced aperture. Bottom: traced aperture with an additional 20 row above and below to account for bleeding from saturated pixels at higher exposure times.*

We measure the sky by calculating the sigma-clipped mean in a small region located in the corners of our custom subarray that is minimally affected by the spectrum signal. We subtract this sky value from the summed counts of the spectrum to account for background noise in the signal.

We calculate the shutter jitter time for each exposure time T:

$$\sigma_t = \frac{\sigma}{\mu} * T, \tag{4}$$

where σ and μ are the standard deviation and the mean of the sum of counts, respectively. We calculate two jitter times using the positive and negative orders separately. For the 2.0-second exposures, timing jitters are calculated for exposures with and without flash separately.

Results

Table 3 in Appendix B presents the rootname, exposure time, shutter blade used, and the sum of counts of the positive orders, negative orders, and the sky for every exposure.

We convert the sum counts in the positive orders into a timing residual for each exposure individually by subtracting the mean for each exposure sequence, i.e. treating the 0.5-s exposures as a set, and the 0.7-s as a set, and so forth, and then dividing by the count rate to convert from counts to a unit of time. We present the results in Figure 5.

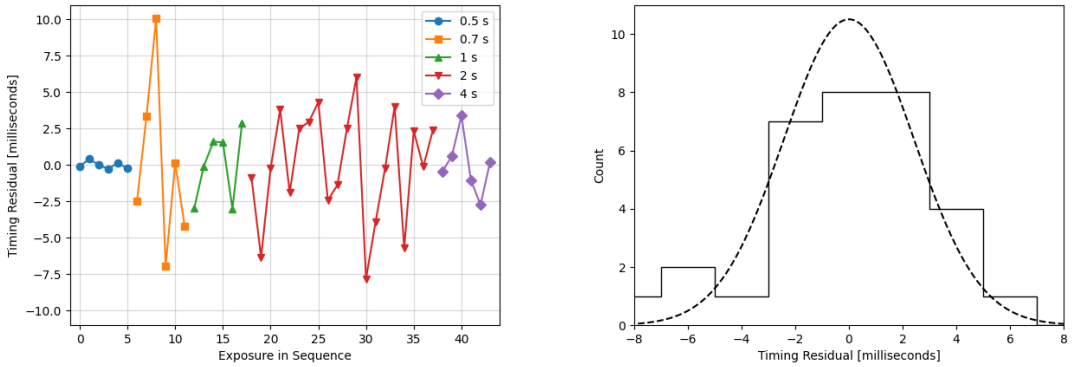

Figure 5: *Left: timing residuals for each exposure in the sequence. Right: the distribution for the set of 32 exposures with nominal times greater than or equal to 1.0-s. A Gaussian with* $\sigma = 2.4$ *milliseconds is plotted for comparison (dashed line). The residuals of the six 0.5-s exposures and the six 0.7-s exposures are much smaller and a bit larger, respectively, than the residuals of the 1.0-s, 2.0-s, and 4.0-s exposures.*

Timing jitters in milliseconds (ms) for positive and negative orders for each exposure time are shown in Table 1. The timing jitter ranges from 0.241 - 5.63 ms, with the largest values from the 0.7-s series. The large timing jitter in 0.7-s exposures may be due to the mechanical vibration affecting the shutter blade's acceleration or deceleration. This vibration typically last for ∼0.7 seconds and has diminishing effects at longer exposures. On the other hand, for 0.5-s exposures the timing jitter is *much smaller* than other exposure times. The ∼10x shorter jitter time may be associated with the unique shutter operation for 0.5-s exposures, in which the shutter blade sweeps continuously without stopping. We also find that the positive and negative orders jitter time are highly correlated, illustrating that the varying shutter time does not also vary across the CCD. Whatever any particular shutter time is for the positive orders, that time also applies to the negative orders.

Table 1: *Jitter time in milliseconds (ms) for each exposure time using the total counts of the positive and negative order spectra, respectively. For 2.0 second exposures, the jitter time is calculated separately for exposures with flash on and off.*

Exposure Time (s)	Jitter (ms) (Positive Order)	Jitter (ms) (Negative Order)	N Exposures
0.5	0.241	0.305	6
0.7	5.519	5.627	6
1.0	2.239	1.932	6
2.0 no flash	3.283	3.272	10
2.0 flash	2.017	2.124	10
4.0	1.846	1.741	6

We calculate the weighted average jitter time using times associated with 1.0-, 2.0-, and 4.0-second exposures. We choose to ignore 0.5- and 0.7-second exposures due to the different nature of these exposures as a consequence of the shutter system. The weighted average jitter time and its uncertainty is calculated using Equations 5 - 7,

$$\overline{\sigma}_t = \frac{\Sigma w_i \sigma_i}{\Sigma w_i}, \tag{5}$$

$$w_i = \frac{1}{u_i^2} = \frac{2(N_i - 1)}{\sigma_t^2} \tag{6}$$

$$\sigma_{\overline{\sigma}_t} = \frac{1}{\sqrt{\Sigma w_i}} \tag{7}$$

where $\overline{\sigma}_t$ and $\sigma_{\overline{\sigma}_t}$ are the weighted average jitter time and its uncertainty, respectively, calculated from the four σ_i in Table 1 for the 1-s, 2-s unflashed, 2-s flashed, and 4-s positive order values and their associated values of N_i (6, 10, 10, and 6, respectively). The weights w_i are equal to the fractional uncertainty of the standard deivation from a finite series ($\frac{u}{\sigma_t}$), calculated from Equation 3. The weighted average jitter time is calculated to be 2.43 $\pm$ 0.32 ms, which is $\sim$4 times shorter than the system requirement of 10 ms.

We also calculated the weighted average jitter time for 1.0-, 2.0- unflashed, and 4.0-second exposures (same measurement as above but only including unflashed exposures), and the *unweighted* average jitter time using 1.0-, 2.0- flashed and unflashed, and 4.0- second exposures. We found that all values are consistent with one another so we report only the one value of 2.43 ms, which is expected given our short dynamic range in our weights (10 measurements for 2-s exposures, 6 measurements for every other exposures).

Shutter jitter calculated using shutter A or B separately are shown in Table 2. They are consistent with the ones derived by combining results from both shutters in Table 1, within the associated errors, which are larger because the number of exposures in each set is halved.

Table 2: *Jitter time in milliseconds for exposures using either shutter A or B separately. Each set has 3 exposures, apart from the two second exposures, which has 5. Results are consistent with each other and with Table 1.*

Shutter A

Exposure Time (s)	Jitter (ms) (Positive Order)	Jitter (ms) (Negative Order)	*N* Exposures
0.5	0.125	0.200	3
0.7	5.350	5.182	3
1.0	2.151	1.802	3
2.0 no flash	2.594	2.468	5
2.0 flash	1.432	1.658	5
4.0	2.515	2.242	3

Shutter B

Exposure Time (s)	Jitter (ms) (Positive Order)	Jitter (ms) (Negative Order)	*N* Exposures
0.5	0.316	0.370	3
0.7	4.356	4.770	3
1.0	1.189	1.423	3
2.0 no flash	3.468	3.495	5
2.0 flash	1.179	1.092	5
4.0	0.692	0.903	3

Figure 6 presents the fractional uncertainty of the shutter jitter and Poisson noise vs the exposure time. The blue points are the weighted average jitter times with associated 1.0-σ uncertainties, from the positive orders of Table 1. The slanted lines are the shutter jitter noise and the Poisson noise as theoretical power laws with indices -1 and -0.5, respectively. The shutter jitter noise dominates Poisson noise for all exposures, and for both, the noise is smaller for longer exposures. The combination (purple line) shows that no accounting is necessary for Poisson noise because it is negligible. Figure 6 also highlights the out-of-family behavior of the 0.5- and 0.7-second exposures associated with the mechanism of the shutter system, as previously mentioned.

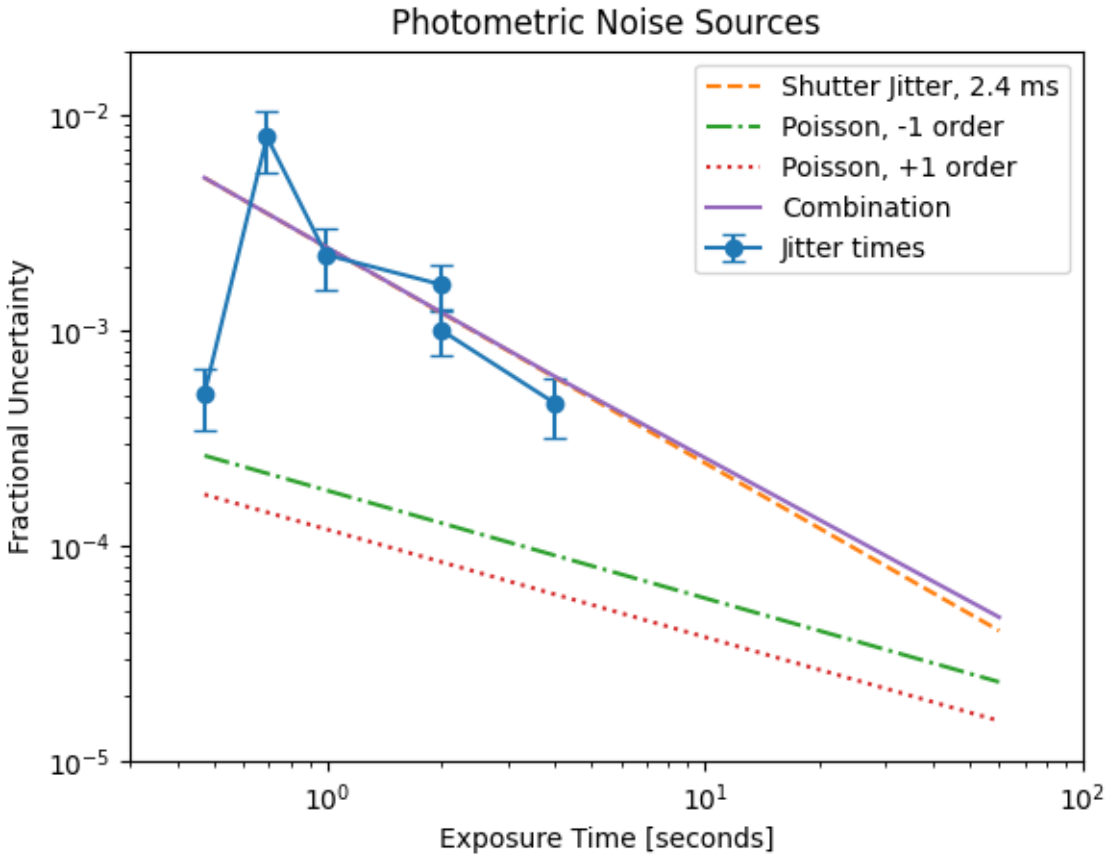

Figure 6: *Photometric noise sources for the sum across the G280 spectra for exposures of various lengths. Two theoretical components, shutter jitter and Poisson noise, are plotted as straight lines with power law indices of -1 and -0.5 respectively. Their root-sum-of-squares combination is also shown. Data from the positive orders in Table 1 are plotted (blue points) with associated 1-σ uncertainties. For comparison, the Poisson noise for a nearly saturated star in a direct image is* $\sim 2 \times 10^{-3}$.

Further Analysis

We plot the positive order count rate, the negative order count rate, and the positive/negative order count ratio in Figure 7. If charge is conserved, we should expect all three plots to be flat. However, this is not the case. We find that as the exposure time increases, the ratio between the positive and negative order count decreases; in particular, the positive/negative order ratios for the 4-s exposures are ∼2% lower than the ratios for the 0.5-s exposures. The periodicity in the 2-s exposures' ratios (Figure 7, right panel) can be explained by the flash level being turned on and off in alternating order for 2-s exposure pairs[9].

[9]The periodicity occurs in pairs of points because of the observing order of the different shutters, i.e. Shutter A unflashed, Shutter B unflashed, Shutter A flashed, Shutter B flashed, etc.

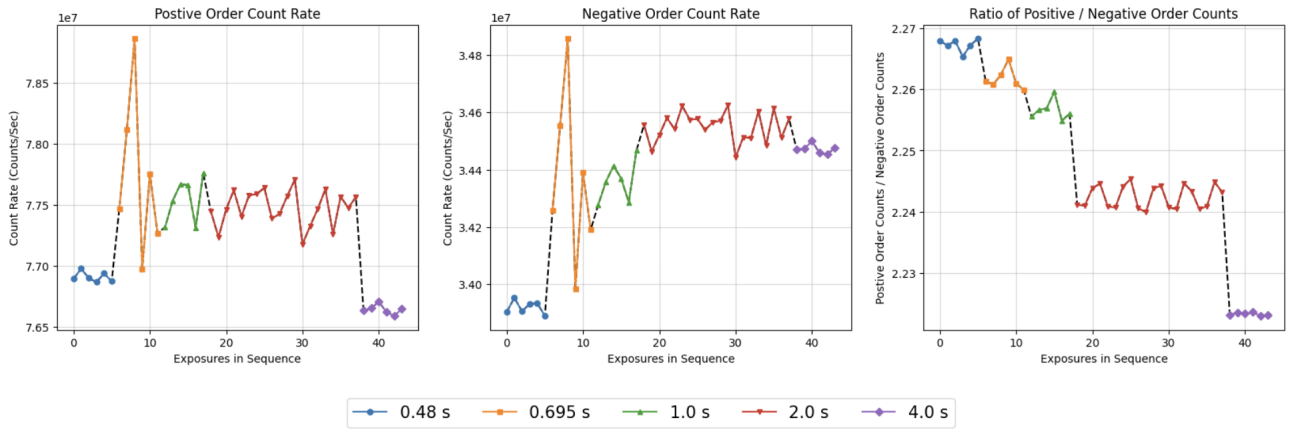

Figure 7: *Positive order count rate (left), negative order count rate (center), and the count ratio between positive/negative order counts (right). As the exposure time increases, the count ratio between the two orders decreases.*

We first investigated effects of saturated pixels bleeding out of the aperture as a potential cause. We experimented with different aperture sizes and different methods to define an aperture such as a box or ellipse that surrounded the spectrum. In all cases, the difference in count ratio were negligible compared to Figure 7. We modified our initial method of measuring the sky (through a small aperture in the corner of each exposures to prevent contamination from the saturated signal, as previously mentioned in the Analysis section) by iterating through different sky calculating algorithms, aperture sizes, and the location of our aperture. In all cases, changing the method of calculating our background had no significant changes in the count ratio in Figure 7.

We then investigate the background noise as a cause of the discrepancy in the ratio plots. Using the HST Exposure Time Calculator (ETC), we estimated the expected sky to be 2.56 e s^{-1} $pixel^{-1}$. Given the high count values for the stellar spectra across all exposures, the background is close to zero and for these high intensity stellar spectra, the background is fairly neglible. However, our "sky" background as measured on the images is negative, ranging from -7.8 e $pixel^{-1}$ to -6.5 e $pixel^{-1}$. We conclude that the negative sky is due to a systematic error in the calibrated images, produced by the `calwf3` pipeline and downloaded from MAST. However, we still suspect that the issues with the background is not the cause for the discrepancy in the postiive-to-negative order ratio due to its small value compared to the stellar flux.

Finally, we did the same analysis on the raw files to determine whether the issue stems from the images' calibration. The total counts in the raw are higher than the flt (calibrated) images due to the nature of `calwf3`'s calibration, however we found the same trends illustrated in Figure 7, eliminating the possibility that the lost counts between each different exposure time is due to the calibration system.

"Drooping": Non-conservation of Charge

Based on Figure 7 we speculate that analog charge is lost in the CCD under saturating conditions. To investigate further, we calculate the sum of the background-subtracted count rate per column in the region of the positive order spectrum for each exposure. We then calculate the average of the resulting column sums for each exposure time. Ideally, the averaged columnwise count rate should be the same between exposure times; i.e. the count rate (in e s^{-1}) in each column in a 4-s exposure should be the same as the count rate in a 0.5-s exposure, and likewise for every other exposure time. However, they are not, in practice.

We ratio the resulting average count rate sum per column for each exposure time against the resulting sum for 0.5-s exposures and plot them against the same 0.5-s exposure sums in Figure 8. We find that the 0.5-s exposure is actually not 0.5-s, but instead is 0.475-s (cf. the next Section), and the 0.7-s exposure is actually 0.695-s. Even after accounting for those actual exposure times, the measured flux is not as expected (Figure 8). The 0.5-s, 0.7-s, and 1-s ratios in the figure are consistent and as expected, i.e. nearly unity across the diagram. However, the flux "droops" at high flux values for 2 and 4 second exposures, where saturation would be the greatest. Notably, for 1E5 e/col in the 0.5-s exposure, the 4-s exposure is $\sim$ 2% lower than unity. We note that the three highest e/col bins in the 2-s data follow the same drooping pattern as the 4-s data, but offset horizontally by a factor of two. Presumably, a given amount of droop occurs at a given level of saturation, such that the saturation level occurs at twice the flux level in the 2-s data than it occurs in the 4-s data.

We do not understand why the 2- and 4-s data are above unity by $\sim$1.5% at low flux levels. We would have expected them to be near unity, similarly to 0.7- and 1-s data. Figure 9 shows the averaged count rate per column ratio between long and short exposures (600/10 seconds) vs the oversaturation level of the longer 600-s exposure as created by Gilliland et al. 2010 (Figure 10 in Gilliland et al. 2010). They found there was a similar positive deviation of 1.8% in the ratio of fluxes at unsaturated flux levels in direct images in UVIS 2.

Furthermore, Figure 9 also exhibits the drooping effect seen in Figure 8. In Figure 9, the flux ratio crosses unity at an oversaturated level of $\sim$30, where the peak of the PSF of the shorter 10-s exposure would have been approximately equal to half of the full well depth by Gilliland's definition of oversaturation. The magnitude of the droop observed by Gilliland was such that even without correction, charge is approximately conserved on UVIS 2. Similarly in Figure 8, drooping begins (i.e. the ratio crosses unity) for 4-s exposures when the 0.5-s exposure is at $\sim$50,000 e^- $column^{-1}$. Thus, our general findings are in rough agreement with Gilliland et al. 2010: charge is approximately conserved on the UVIS 2 CCD, even for saturating exposures. Addressing the small (+/-2%) deviations from ideal photometric performance is beyond the scope of this report.

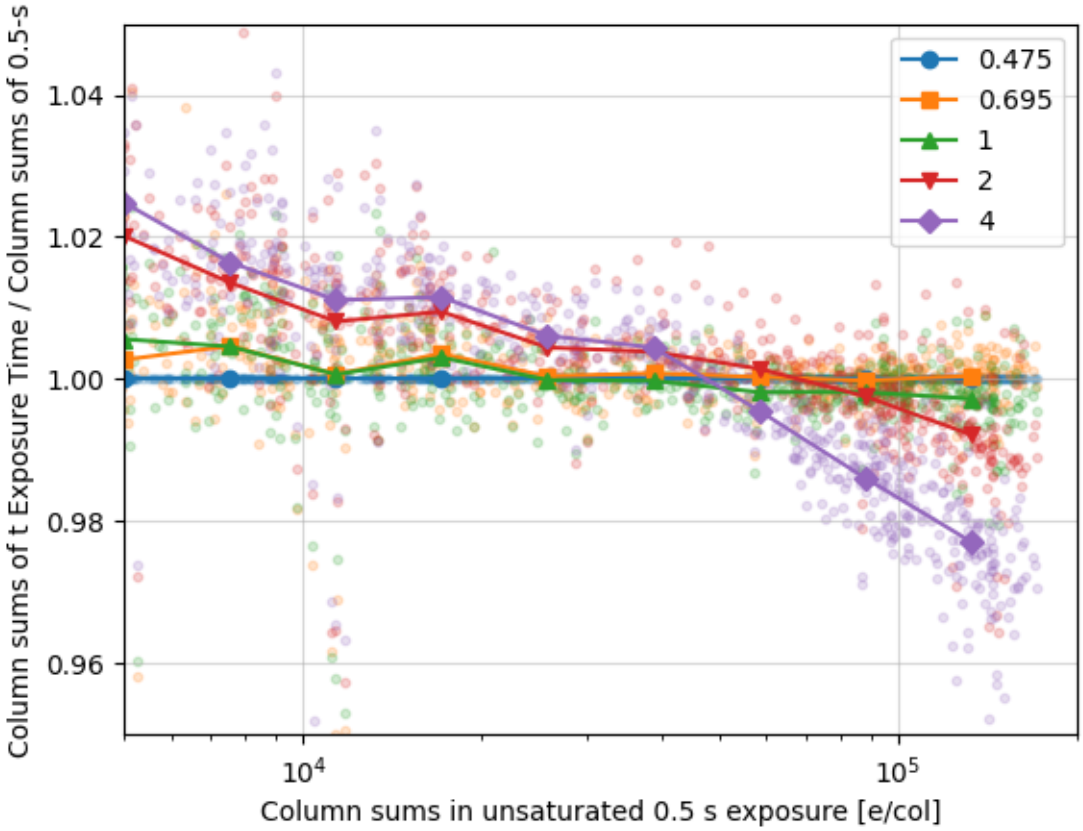

Figure 8: *Sum of counts over all columns for each exposure time normalized to the 0.5-s exposure plotted vs. column sums of the 0.5-s exposure. Numerous semi-transparent points correspond to individual columns in the positive orders; solid points connected by lines are binned values, logarithmically spaced. Points are colored purple, red, green, orange, and blue for 4-s, 2-s, 1-s, 0.7-s, and 0.5-s, respectively. The 0.5-s ratio is unity by definition. The exposure times in the legend are the measured times in seconds, not the commanded times.*

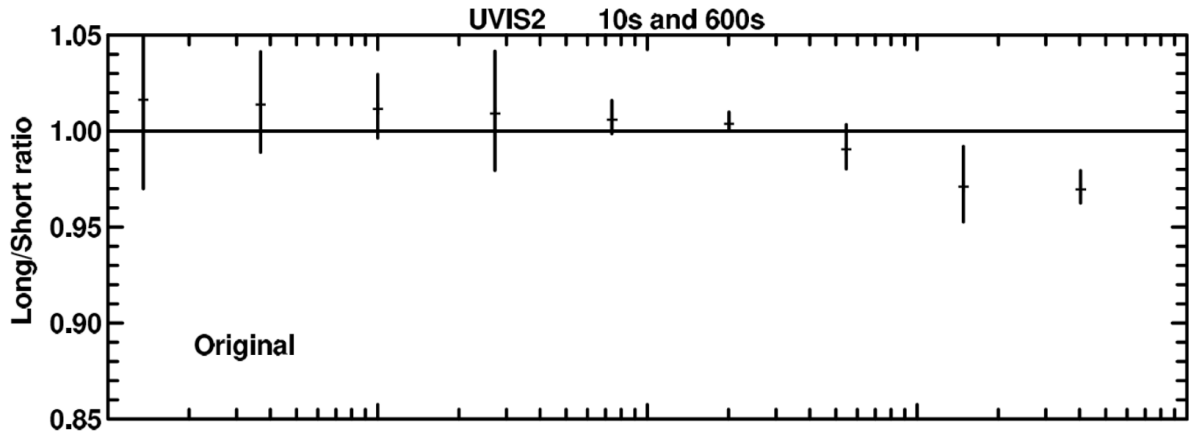

Figure 9: *Adapted from Figure 10 of Gilliland et al. 2010. Ratios of the long to short exposure sums (600-s/10-s) normalized by the exposure time ratio in natural log intervals of the over-saturation level of the long exposure (600-s) in UVIS 2. Similar to Figure 8, one to two percent deviations above unity occur at levels below saturation and two to three percent deviations below unity occur far above saturation.*

Commanded vs. Actual Exposure Time

We investigate any disparities between the commanded exposure time vs. actual exposure time of our exposures. If the actual exposure time differed from what is commanded, this may affect the calculated count rates and explain the discrepancies seen in Figure 7. This is especially true for lower exposure times, as the difference between commanded vs. actual is less prominent at longer exposures.

The 0.48-s and 0.695-s values for commanded exposure times of 0.5 s and 0.7 s respectively both originated with Hilbert's analysis of direct images of the standard star GD153 through filter F395N obtained in Program 11427.[10] For that report's 22 measurements with commanded exposure times of 0.5-s, the mean measured exposure time was 0.480 ± 0.0027 s.

We used reduced data from Program 11427 by Sahu et al. 2015 and Sahu (private communication) to estimate the ratio of fluxes of GD153 in (nominally) 0.5-s and 1.0-s exposures, and from this, estimate an actual value exposure time of 477 ± 3.8 milliseconds rather than 500 milliseconds. Using data similar to Program 11427 from Program 14019 (Sahu, private communication), we estimate an exposure time of 479 ± 5.4 milliseconds. The larger uncertainty of the Program 14019 data is due to fewer measurements (22 for Program 11427 vs 15 for Program 14019).

We made the same calculation by dividing the mean count of the 0.5-s exposures by the mean count of the 1.0-s exposures using G280's negative and positive orders separately. Our estimates for the actual commanded exposure time for the 0.5-s exposure is 474 ± 0.8 ms using the negative order counts (where no pixels are saturated) and 476 ± 0.9 ms using the positive order counts (in which the 1.0-s exposures were saturated). The two values are in

[10]Implemented in 2010 via PR PR65349 / OPUS-65349.

agreement with each other (within $\sim 2\sigma$) and with the GD153 data of Programs 11427 and 14019, within the associated uncertainties.

We recalculated the count rates of 0.5-s exposures using the average of the two calculated exposure time derived from G280's spectrum (0.475-s) instead of the commanded exposure time (0.480-s). We find that the new count rates are in family with 1- and 2-s exposures, differing by 0.002-0.003%[11]. However, we do not conclude whether or not the 0.48-s value that populates the FITS headers should be modified to 0.475 (a 1% decrease) because 0.48-s is still consistent within the uncertainties of our data.

The larger shutter timing jitter of the 0.7-s exposure has affected only a small number of programs. As seen in Table 4 in Appendix C, For external exposures with commanded times of 0.7, we count 35 GO programs, 276 calibration programs, and 4 internal flat fields.

Secular Shift of the G280 Spectrum

We noticed a secular shift in all of our G280 spectrum's X position, i.e. parallel to the dispersion, totalling $\sim$0.01 arcsecond across the twenty 2-s exposures accumulating in a roughly linear fashion. The shift presumably occurs throughout the visits; it is also apparent in the 4-s series but is less clear in the others. We did not search for shifts in the spectrum's Y position.

We speculate that the shift is due either to A) a pointing control software error somehow affecting only data from the UVIS grism, perhaps via correction of differential velocity aberration, or B) a mechanical effect, such as the shutter vibration shaking the filter wheel that holds the G280 element from its nominal position at its electromechanical detent. Neither seems plausible, *e pur si muove* (and yet it moves).

Although the shift is quite noticeable in regions of the spectrum with large gradients, it has no effect on our analysis of the timing jitter. Further analysis is beyond the scope of this report.

Conclusions

We determined the timing jitter of the UVIS shutter from G280 spectra taken in a single HST orbit. The exposure time varies by 2.43 ± 0.32 milliseconds r.m.s. for nominal exposure times greater than or equal to 1 second. This value meets the system requirement of 10 ms repeatability, and is in fact $\sim$4 times smaller than the system requirement. The jitter necessarily produces a $\sim$0.24% photometric error for a 1-s exposurse, and as such should be included in the noise budget for precise (non-differential) photometry in short exposures, because it is comparable to the Poisson error of a nearly saturated star exposed for 1 second in a direct image with WFC3 UVIS.

We measure a 5.51-s timing jitter in 0.7-s exposures, which is more than double our reported r.m.s. value, and speculate that it may be caused by vibrations associated with shutter operation interacting poorly with the torques on the shutter during its acceleration or deceleration. Contrariwise, we measure a 0.241 timing jitter for 0.5-s exposures, which is $\sim$ 10 smaller than our reported value. Its out-of-family and improved performance may be

[11] We choose to ignore the 4.0-s exposures due to its out of family behavior seen in Figure 7.

associated with the shutter mechanism for consecutive 0.5 second exposures; in which the shutter blade continuously sweeps without stopping, avoiding one potential source of jitter. Because of the much smaller timing jitter for 0.5-s exposures than 0.7-s exposures, observers should consider substituting a 0.5-s exposure whenever a 0.7-s exposure otherwise would be indicated, although this recommendation is only based on a dozen exposures taken in series (six 0.5-s and six 0.7-s).

Both this study and a simple analysis of bowtie flats' repeatability presented in Figure 10 in Appendix A contradict some prior studies that measured much larger shutter timing jitter, in particular Hilbert 2004, Hilbert 2010, and Sahu et al. 2015 (WFC3 ISR 2004-14, ISR 2009-25, and ISR 2015-12). The possibility that the shutter's behavior has changed over the years could be investigated and might explain this potential contradiction.

Acknowledgements

We appreciate the additional orbit allocated by the Hubble Mission Office which enabled this work after a observing error ruined the first visit. The authors wish to thank Jennifer Mack, Sylvia Baggett, and Debopam Som for advice on program preparation and data analysis. We also thank Mariarosa Marinelli, Annalisa Calamida, and Joel Green whose review improved this report. We also used OpenAI's ChatGPT (GPT 3.5) for tutoring in Python.

References

Gilliland, R. L., A. Rajan, and S. Deustua (Oct. 2010). *WFC3 UVIS Full Well Depths, and Linearity Near and Beyond Saturation*. Instrument Science Report WFC3 2010-10, 21 pages.

Hilbert, B. (Dec. 2004). *Stability and Accuracy of the WFC3 UVIS Shutter*. Instrument Science Report WFC3 2004-14, 15 pages.

— (2010). *WFC3 SMOV Program 11427: UVIS Channel Shutter Shading*. Instrument Science Report WFC3 2009-25, 22 pages.

Kurtz, H., P. R. McCullough, and S. Baggett (Aug. 2018). *UVIS Flat Fields Affected by Shutter-Induced Vibration*. Instrument Science Report WFC3 2018-11, 20 pages.

Miles, Nathan D. et al. (Sept. 2021). "Using Cosmic Rays Detected by HST as Geophysical Markers. I. Detection and Characterization of Cosmic Rays". In: 918.2, 86, p. 86. DOI: 10.3847/1538-4357/abfa9b. arXiv: 2006.00909 [astro-ph.IM].

Sahu, Kailash, C. M. Gosmeyer, and Sylvia Baggett (July 2015). *WFC3/UVIS Shutter Characterization*. Instrument Science Report WFC3 2015-12, 11 pages.

Appendix A: Bowties

We examined "bowtie" flat fields, i.e. internal flat fields taken regularly for years, limiting our analysis to 1-s exposures taken with shutter position A, and dividing by a reference bowtie flat. By selecting a time period in which long-term trends and anomalies were insignificant, by eye, specifically from Dec 8, 2014 to Sep 3, 2017, we established a set of 173 nearly-identical flat fields illuminated by the internal tungsten lamp (Figure 10). We interpret the standard deviation (0.0035) of the ratio image medians as an upper limit on the shutter timing jitter of < 3.5 milliseconds (for 1-s exposures). It's an upper limit because shutter timing jitter is not the only contributing factor in the variation of the median measured brightness of an internal flat field: the vibration associated with shutter operation could be affecting the brightness of the lamp or its throughput to the detector via the calibration subsystem (Kurtz et al. 2018). Poisson and read noise are insignificant for the medians of these full-frame images, which have millions of pixels and ∼10,000 e-/pix after 3x3 binning on chip (Kurtz et al. 2018, Section 2.1). Analyzing the 500+ F645N flat fields accrued on orbit, accounting for varied exposure times between 1 and 5 seconds, would be a useful study but is beyond the scope of this work.

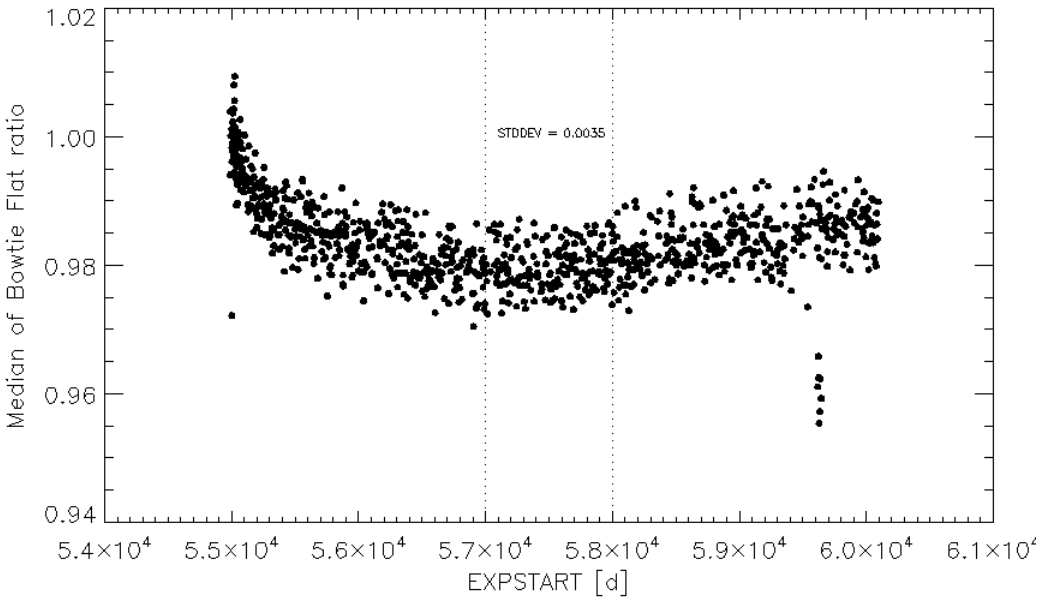

Figure 10: *Medians of 976 bowtie flat fields normalized to a reference one, iac70adfq, from launch to the present (2009-2023). The standard deviation of the 173 values between the dotted vertical lines is 0.0035.*

Appendix B

Table 3: *The total sum counts for the positive and negative order spectras in units of ten million counts, sky values (e-/pixel), and metadata (rootname, exposure time, and shutter blade positioning) of all 44 exposures. Exposures with an asterisk are post-flashed at a commanded level of 20 electrons per pixel.*

Rootname	Exptime (s)	Shutter	+Sum (e+07 Counts)	-Sum (e+07 Counts)	Sky (e-/pixel)
if2r02agq	0.5	A	3.6908	1.6273	-7.86
if2r02ahq	0.5	B	3.6948	1.6297	-8.81
if2r02aiq	0.5	A	3.6911	1.6275	-7.96
if2r02ajq	0.5	B	3.6895	1.6287	-7.91
if2r02akq	0.5	A	3.6930	1.6289	-7.90
if2r02alq	0.5	B	3.6898	1.6267	-7.83
if2r02amq	0.7	A	5.3841	2.3809	-7.76
if2r02anq	0.7	B	5.4292	2.4015	-8.10
if2r02aoq	0.7	A	5.4809	2.4226	-7.48
if2r02apq	0.7	B	5.3496	2.3620	-7.51
if2r02aqq	0.7	A	5.4040	2.3901	-7.43
if2r02arq	0.7	B	5.3700	2.3762	-7.32
if2r02asq	1.000	A	7.7317	3.4278	-8.00
if2r02atq	1.000	B	7.7534	3.4358	-6.69
if2r02auq	1.000	A	7.7667	3.4413	-7.53
if2r02avq	1.000	B	7.7660	3.4369	-7.53
if2r02awq	1.000	A	7.7312	3.4286	-7.22
if2r02axq	1.000	B	7.7759	3.4467	-7.21
if2r02b4q	2.000	A	10.5489	6.9113	-7.09
if2r02b5q	2.000	B	10.5447	6.8927	-7.35
if2r02b6q *	2.000	A	10.5492	6.9043	-7.28
if2r02b7q *	2.000	B	10.5524	6.9161	-6.99
if2r02b8q	2.000	A	10.5481	6.9082	-7.17
if2r02b9q	2.000	B	10.5515	6.9245	-7.96
if2r02baq *	2.000	A	10.5517	6.9148	-6.65
if2r02bbq *	2.000	B	10.5528	6.9154	-8.05
if2r02bcq	2.000	A	10.5477	6.9077	-7.33
if2r02bdq	2.000	B	10.5485	6.9131	-7.86
if2r02beq *	2.000	A	10.5514	6.9141	-6.16
if2r02bfq *	2.000	B	10.5541	6.9250	-7.63
if2r02bgq	2.000	A	10.5435	6.8886	-6.98
if2r02bhq	2.000	B	10.5465	6.9026	-7.19
if2r02biq *	2.000	A	10.5493	6.9021	-6.59

Continued on next page

Rootname	Exptime (s)	Shutter	+Sum (e+07 Counts)	-Sum (e+07 Counts)	Sky (e-/pixel)
if2r02bjq *	2.000	B	10.5525	6.9207	-7.50
if2r02bkq	2.000	A	10.5452	6.8968	-7.22
if2r02blq	2.000	B	10.5513	6.9227	-6.87
if2r02bmq *	2.000	A	10.5495	6.9022	-5.47
if2r02bnq *	2.000	B	10.5512	6.9154	-7.51
if2r02ayq	4.000	A	30.0652	10.3788	-6.52
if2r02azq	4.000	B	30.0660	10.3789	-5.87
if2r02b0q	4.000	A	30.0682	10.3800	-6.35
if2r02b1q	4.000	B	30.0648	10.3783	-6.53
if2r02b2q	4.000	A	30.0635	10.3781	-6.54
if2r02b3q	4.000	B	30.0658	10.3790	-6.46

Appendix C

Table 4: *Total number of times a specific short exposure time is used for GO, calibration, and internal flat field programs on the UVIS detector. In this report, the largest shutter timing jitter is associated with 0.7-s exposures, in bold below.*

Exposure Time Used (s)	GO	Calibration	Internal Flat Fields
0.5	842	872	442
0.7	**35**	**276**	**4**
0.8	82	187	0
0.9	28	77	0
1.0	545	978	4247